Int. J. Heat Mass Transfer. Vol. 36, No. 13, pp. 3171–3186, 1993
Printed in Great Britain

0017–9310/93 $6.00+0.00

The melting process of ice from a vertical wall with time-periodic temperature perturbation inside a rectangular enclosure

C. J. HO† and C. H. CHU
Department of Mechanical Engineering, National Cheng Kung University, Tainan, Taiwan 701, R.O.C.

(*Received* 7 *October* 1992 *and in final form* 18 *February* 1993)

Abstract—A numerical investigation of natural-convection-dominated melting process of ice from a vertical wall of a square enclosure is reported. Time-dependent sinusoidal temperature perturbation is imposed on the vertical hot wall of the enclosure, and its effects on the heat transfer and buoyancy-driven flow during the melting process of ice are examined. For all the simulations conducted in the present study, a steady periodic melting regime at a frequency of the imposed time-periodic temperature perturbation emerges following a period of transient oscillatory melting process. The synchronous response of the melting process of ice to the imposed time-periodic perturbation on the hot wall temperature is found to be strongly affected by the density inversion phenomenon of water. Parametric simulations have been performed to unveil the effects of the relevant parameters on the heat transfer characteristics during the steady periodic melting regime of ice inside the enclosure. Results clearly demonstrate the feasibility of controlling the melting heat transfer in an ice-filled enclosure by means of the time-periodic perturbation of the wall temperature in conjunction with the density inversion phenomenon of water near 4°C.

INTRODUCTION

IN VIEW of its fundamental importance in a wide range of technological applications as well as the naturally occurring phenomena, the heat transfer problem of melting of a phase change material (PCM) from a vertical hot wall inside a rectangular enclosure has been investigated extensively as revealed in the literature reviews given by Viskanta [1–3]. As demonstrated in previous works [4–8], knowledge of buoyancy-driven flow in the melt region is vital for making an accurate description of the melting heat transfer process from a vertical wall of isothermal temperature or constant heat flux. It can be further noted that the thermal boundary conditions of the hot vertical surface considered in the early literature of the natural-convection-dominated melting problem are time-independent isothermal or constant-heat-flux, with the exception of our recent study [9] in which numerical simulations have been performed for melting process of a pure metal (tin) from an isothermally heated vertical wall subjected to a time-periodic temperature perturbation inside a vertical square enclosure. A steady periodic melting behavior with a frequency equal to that of the imposed time-periodic perturbation on the hot wall temperatures arises following a period of transient oscillatory melting process. The steady periodic mean values of the heat transfer rates as well as the melted fraction are approximately equal to those under a static wall temperature at the mean value of the sinusoidal perturbation; and they are strongly affected by the Rayleigh number and the subcooling parameter, but rather insensitive to the oscillation amplitude or the time period of the imposed surface temperature perturbation. The present work is an extension of the earlier study [9]. A physical configuration identical to the previous work [9] but filled with ice as the solid PCM is considered here, representing our continuing effort to explore the influence of cyclic temporal temperature perturbation of the heated wall on the natural-convection-dominated melting process in a vertical enclosure. Moreover, to further improve the computational efficiency, a numerical algorithm different from that used in the earlier study [9] has been devised.

For the melting process of ice from a vertical surface inside a rectangular enclosure as illustrated schematically in Fig. 1, it is rather surprising to find from the literature survey that little or no previous study dealing with this configuration exists; the existing literature concerning heat transfer during the melting process of ice in a confined space appears to be mostly restricted to the geometry of a cylinder or cylindrical annulus as indicated by the representative works [10–14]. These studies were primarily motivated by the feasible applications of ice thermal storage techniques for the air-conditioning of large buildings. It has been established that the density anomaly of water in the vicinity of the melting point of ice can exert strong influence on the heat transfer characteristics during the melting process of ice in enclosures. All these studies were focused on the melting process of ice under time-independent thermal boundary conditions. However, in practical applications the boundary conditions may

† To whom correspondence should be addressed.

NOMENCLATURE

a	amplitude of oscillatory surface temperature
A	dimensionless amplitude of oscillatory surface temperature, $a/(\bar{T}_h - T_f)$
$A_{q,c}$	oscillatory amplitude of Q_c
$A_{q,h}$	oscillatory amplitude of Q_h
A_r	oscillatory amplitude of V^*
Ar	aspect ratio, W/H
b	exponent of density equation
c_p	specific heat
f^+	frequency
f	dimensionless frequency, f^+H^2/α_l
Fo	Fourier number, $\alpha_l t/H^2$
g	gravitational acceleration
H	height of enclosure
k	thermal conductivity
L	latent heat
p	dimensionless time period, $1/f$
Pr	Prandtl number, ν_l/α_l
$\bar{q}$	average heat flux at vertical wall
Q	dimensionless heat transfer rate
R	density inversion parameter, $(T_m - T_f)/(\bar{T}_h - T_f) = Ste_m/Ste$
Ra	Rayleigh number, $g\,rsp\,\lvert\bar{T}_h - T_f\rvert^b H^3/(\alpha_l \nu_l)$
rsp	coefficient of density equation
S	dimensionless position of solid–liquid interface
Sc	subcooling factor, $(T_f - T_c)/(\bar{T}_h - T_f)$
Ste	Stefan number, $c_{p,l}(\bar{T}_h - T_f)/L$
Ste_m	reference Stefan number, $c_{p,l}(T_m - T_f)/L$
t	time
T	temperature
V_m	volume of liquid PCM
V_0	total volume of PCM
V^*	volumetric fraction of liquid PCM, V_m/V_0
W	width of enclosure
x^+, y^+	Cartesian coordinates
x, y	dimensionless coordinates, $x^+/H, y^+/H$.

Greek symbols

α	thermal diffusivity, $k/(\rho c_p)$
θ	dimensionless temperature, $(T - T_f)/(\bar{T}_h - T_f)$
ν	kinematic viscosity
ξ	dummy variable
ρ	density
ψ^+	steam function
ψ	dimensionless stream function, ψ^+/α_l
ω^+	vorticity
ω	dimensionless vorticity, $\omega^+ H^2/\alpha_l$.

Subscripts

c	cold surface
f	fusion point
h	hot surface
l	liquid phase
m	maximum density
s	solid phase.

Superscripts

*	ratio of quantity for solid to that for liquid phase
—	average value.

not be fixed in time. Moreover, the influence of time-dependent boundary condition is of interest in connection with the feasibility and means of controlling heat transfer through boundary perturbations. Therefore, the primary objective of the present study is to investigate via a finite difference simulation the heat transfer characteristics of the natural-convection-dominated melting process of ice from a vertical wall modulated with time-dependent sinusoidal surface temperature within a square enclosure, thereby exploring the feasibility of controlling the melting heat transfer in an ice-filled enclosure by means of time-periodic perturbation of the wall temperature.

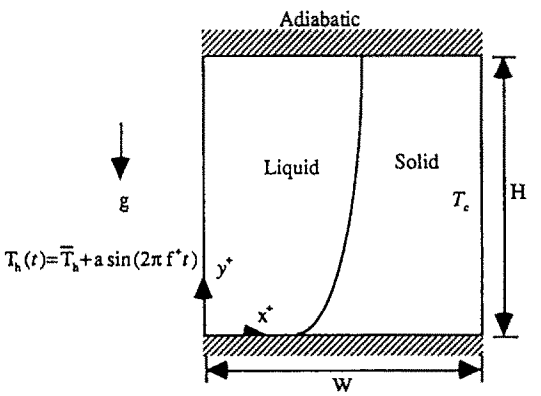

FIG. 1. Schematic diagram of physical configuration and coordinate system.

PROBLEM STATEMENT AND MATHEMATICAL FORMULATION

The two-dimensional melting process from a vertical wall with time-dependent sinusoidal surface temperature inside an enclosure as depicted in Fig. 1 is identical to that considered in ref. [9] except that ice is the solid PCM. There is thus no need to repeat the detailed problem statement and the physical assumptions here. In short, the dimensionless govern-

ing differential equations for the melting process considered can be expressed in terms of stream function, vorticity, and temperature as follows:

In the water region:

$$\frac{\partial \omega}{\partial Fo} + \frac{\partial \psi}{\partial y}\frac{\partial \omega}{\partial x} - \frac{\partial \psi}{\partial x}\frac{\partial \omega}{\partial y} = Pr\nabla^2\omega + Pr\,Ra\frac{\partial |\theta - R|^b}{\partial x} \quad (1)$$

$$\nabla^2\psi = -\omega \quad (2)$$

$$\frac{\partial \theta}{\partial Fo} + \frac{\partial \psi}{\partial y}\frac{\partial \theta}{\partial x} - \frac{\partial \psi}{\partial x}\frac{\partial \theta}{\partial y} = \nabla^2\theta. \quad (3)$$

In the ice region:

$$\frac{\partial \theta}{\partial Fo} = \alpha^*\nabla^2\theta. \quad (4)$$

Here the nonlinear density–temperature relation of water is described using the correlation proposed by Gebhart and Mollendorf [15] of the form

$$\rho = \rho_m(1 - rsp|T - T_m|^b) \quad (5)$$

where $\rho_m (= 999.972\ \text{kg m}^{-3})$ is the maximum density, $rsp = 9.297173 \times 10^{-6}\ (^\circ\text{C})^{-b}$, $T_m = 4.0293^\circ\text{C}$ and $b = 1.894816$. The dimensionless initial/boundary conditions for the present problem are:

$$\text{at } Fo = 0;\quad \psi = \omega = 0,\quad \theta = -Sc,\quad \text{and} \quad (6)$$

for $Fo > 0$;

$$y = 0 \text{ and } 1,\quad 0 \leqslant x \leqslant Ar;\quad \psi = \frac{\partial \theta}{\partial y} = 0 \quad (7a)$$

$$x = 0,\quad 0 \leqslant y \leqslant 1;\quad \psi = 0, \theta = 1 + A\sin\left(\frac{2\pi Fo}{p}\right) \quad (7b)$$

$$x = Ar,\quad 0 \leqslant y \leqslant 1;\quad \theta = -Sc. \quad (7c)$$

At the solid–liquid interface, the continuity of temperature and the energy balance lead to

$$\theta = 0, \text{ and } \left[1 + \left(\frac{\partial S}{\partial y}\right)^2\right]\left(k^*\frac{\partial \theta}{\partial x}\bigg|_s - \frac{\partial \theta}{\partial x}\bigg|_l\right) = \frac{\rho^*}{Ste}\frac{\partial S}{\partial Fo}. \quad (7d)$$

SOLUTION METHODOLOGY

The model equations of the problem were solved numerically using a finite difference method. The spatial derivatives were discretized employing the second-order central differencing scheme except for the convective terms for which the second-upwind scheme [16] was adopted. The temporal derivatives were approximated by means of the forward differencing. In order to improve computational efficiency in solving the phase change problem under consideration, a solution methodology somewhat different from the enthalpy formulation used in the previous work [9] was devised. In general, the solution methodology for solving the solid–liquid phase change problem can be classified into two approaches: the fixed grid [9, 17, 18] and the transformed grid [5–7, 12, 13] methods. The former is used in the enthalpy formulation, in which a fixed grid is laid over the entire PCM domain and the latent heat release/absorption at the interface is accounted for by introducing a source term in the energy equation; while the latter is primarily adopted for the one immobilizing the moving interface via a suitable coordinate transformation and then solving for temperature distributions in the solid and liquid regions, separately. The solution methodology developed in the present work can be viewed somewhat as a hybrid algorithm of these two approaches; namely, the temperature field is solved separately for the solid and liquid regions but on a fixed grid over the entire PCM domain. The solution procedure is based on the quasi-stationary approximation [5] in which the location of the moving solid–liquid interface is explicitly determined using the energy balance equation, equation (7d). Similar to the transformed grid method, an initial position of the solid–liquid interface is prerequisite to initiate the present solution procedure. To this end, the initial position of the phase-change front is determined by incorporating the enthalpy formulation as that employed in refs. [9, 17, 18] for the first time step of the simulation. This is different from that commonly adopted in the transformed grid approach [5–8, 12, 13] using an estimated initial melt thickness. With the obtained initial melt thickness, the solution procedure then proceeds similar to that of the transformed grid approach but on a fixed grid system. The spatial discretization of the differential equations for the grids adjacent to the solid–liquid interface was carried out by means of suitable polynomial interpolation [19]; and the boundary treatments for the buoyant flow calculations at the interface followed those described in refs. [17, 18]. At each time step, the flow field in the liquid region as well as the temperature distributions in both solid and liquid regions were calculated implicitly through a line relaxation scheme. The iteration was continued until a relative convergence criteria of 10^{-4} was met by all the field variables of the problem.

The above-elaborated solution methodology was validated by performing calculations for the problem of melting of pure tin from a time-independent isothermal vertical surface in a shallow enclosure; and as shown in Fig. 2, comparisons were made with the data available in refs. [20, 21] and the results form our earlier study [9] as well. A favorable agreement between the results from the present algorithm and those of refs. [9, 20] can be readily observed in Fig. 2, lending validation for the solution algorithm developed in this study. In addition, in terms of the computational efficiency, the calculation for this case using the present solution algorithm required less than half of the CPU time consumed by the enthalpy formulation adopted in ref. [9]. Furthermore, the vali-

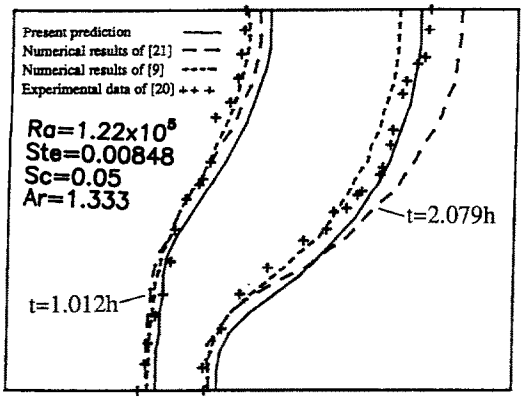

FIG. 2. Comparison of the predicted melting fronts of pure tin in a rectangular cavity with the existing data.

dation calculations using the present algorithm have also been performed for the problem of freezing of water inside a rectangular cavity considered in ref. [22]. In comparison of the isotherm distributions obtained with that provided in ref. [22] (not shown here), a reasonable agreement was obtained, confirming the validity of the present algorithm in solving the natural-convection-dominated phase change problem in the presence of density anomaly.

A series of preliminary calculations for the grid-size study has been carried out as exemplified in Fig. 3 displaying the convergence of the extreme values of the stream function with the grid size during a melting process of ice. Two uniform grid systems were used for the calculations, mainly depending on the Stefan number: 41×41 for $Ste = 0.051$ and 51×51 for $Ste = 0.101$. Also shown in Fig. 3 are the results for the convergence test of varying time step; and a time step of 1.25×10^{-3} was used for the calculations except for the cases of $p = 0.25$ where a smaller time step of 6.25×10^{-4} was found to be appropriate.

RESULTS AND DISCUSSION

Numerical simulations were carried out for the melting process of ice in a square enclosure ($Ar = 1$)

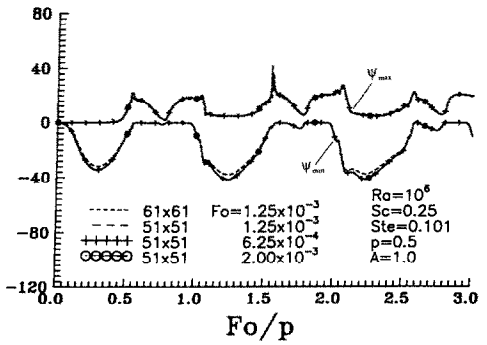

FIG. 3. Convergence tests of the extreme values of stream function with grid-size and time-step.

with a time-dependent sinusoidal hot wall temperature having the relevant dimensionless parameters in the following ranges: the Stefan number $Ste = 0.051$ ($\bar{T}_h = 4°C$) and 0.101 ($\bar{T}_h = 8°C$), the subcooling parameter $Sc = 0.25$–1.5, the Rayleigh number $Ra = 10^4$–10^6, the dimensionless time period of the wall temperature oscillation $p = 0.25$–2.0, and the dimensionless amplitude of the wall temperature oscillation $A = 0$–1.0. Typically, more than six hours of CPU time on VAX-9420 computer were necessary for a simulation to reach a fully developed steady periodic melting regime of ice in the enclosure.

Similar to the findings in ref. [9] for pure tin as the PCM, in all the calculations conducted in the present work, a steady periodic melting regime of ice under the time-periodic hot-surface temperature perturbation emerges after an initial oscillatory melting process. During the steady periodic melting regime, the melted fraction of ice as well as the heat transfer rates through the thermally active wall of the enclosure exhibits a synchronous response to the imposed time-periodic perturbation of the surface temperature. The presentation of the present results will primarily focus on the parametric effects of A, p, Ra and Sc under two different values of Ste on the heat transfer characteristics as well as the melted fraction during the steady periodic melting regime of ice inside the enclosure.

Effect of oscillation amplitude

The synchronous response of the melting process of ice to varying amplitude of the hot-wall temperature oscillation is found to be a strong function of the Stefan number, namely the density inversion parameter R. Figure 4 displays the histories of the volumetric melted fraction (V^*) and the average dimensionless heat transfer rates at the hot and cold walls ($\bar{Q}_h$ and $\bar{Q}_c$) of the enclosure for $Ste = 0.051$ ($\bar{T}_h = 4°C$), $Sc = 0.25$, $Ra = 10^6$, and $p = 0.5$ with varying oscillation amplitude of the hot wall temperature. The local and average dimensionless heat transfer rates through the hot and cold walls of the enclosure are, respectively, defined as

$$Q_h = -\left.\frac{\partial \theta}{\partial x}\right|_{x=0} = \frac{q_h H}{k_f(\bar{T}_h - T_f)} \tag{8a}$$

$$Q_c = \left.\frac{\partial \theta}{\partial x}\right|_{x=Ar} = \frac{q_c H}{k_s(\bar{T}_h - T_f)} \tag{8b}$$

and

$$\bar{Q}_h = \int_0^1 Q_h \, dy = \frac{\bar{q}_h H}{k_f(\bar{T}_h - T_f)} \tag{9a}$$

$$\bar{Q}_c = \int_0^1 Q_c \, dy = \frac{\bar{q}_c H}{k_s(\bar{T}_h - T_f)}. \tag{9b}$$

From an overview of the figure, one can notice that the average heat transfer rate at the hot wall $\bar{Q}_h$ exhibits a steady cyclic variation first, the melted fraction V^*

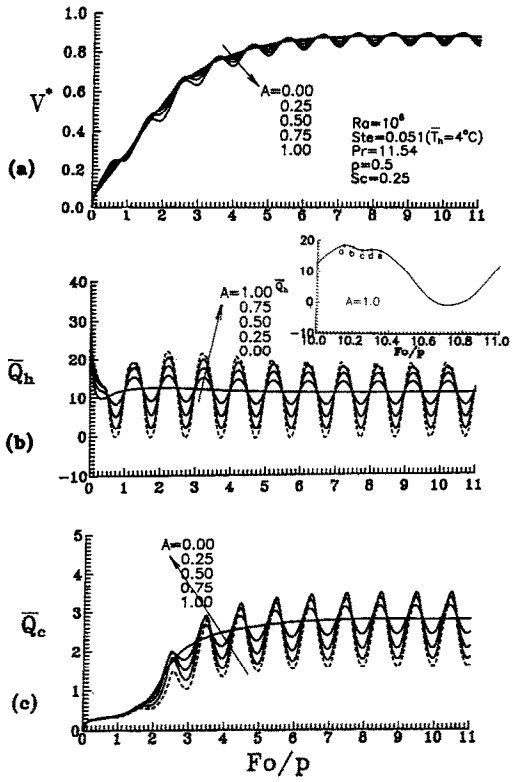

FIG. 4. Effect of oscillation amplitude on temporal variations of melted fraction of ice and heat transfer rates at the vertical walls for $Ste = 0.051$.

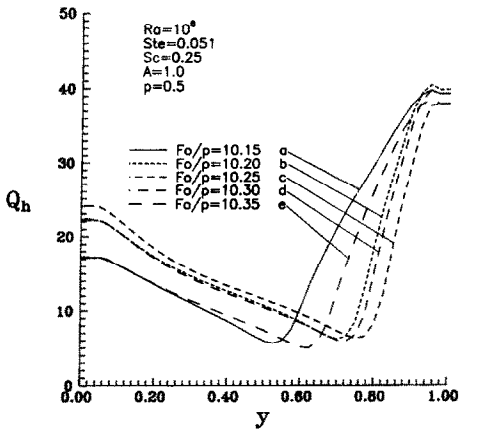

FIG. 5. Variations of local heat transfer profile at the hot wall.

second, and the average heat transfer rate through the cold wall $\bar{Q}_c$ last. The damping effects of the phase change process on the penetration of the temporally cyclic perturbation on the hot wall across the enclosure can be readily inferred from the delay of $\bar{Q}_c$ reaching the steady periodic oscillation with much smaller amplitude than that of $\bar{Q}_h$, as shown in Fig. 4. The increase of the amplitude of the imposed surface temperature oscillation appears to induce increasingly oscillatory behavior of the heat transfer rates and the melted fraction. In addition, the increase of the forcing oscillation amplitude results in a marked decrease of the local minimum values of the melted fraction and the average heat transfer rates during the steady periodic melting regime. From a closer examination of Fig. 4(b), it can be detected that the cyclic variation of the heat transfer rate at the hot wall for $A = 1.0$ as compared with those under the lower amplitudes $A \leqslant 0.75$ displays a rather peculiar crest shape featuring a local minimum at the end of the first quarter of the cycle as shown in the inset of the figure. The occurrence of such peculiarity may be rationalized by examining evolution of the local heat transfer profile on the hot wall over the corresponding time interval, as plotted in Fig. 5 for $A = 1.0$. The curves presented in Fig. 5 clearly demonstrate the non-monotonic variation in local heat transfer rate at the hot wall with position as well as with time. The local heat transfer distribution features a gradual decline from the bottom of the surface reaching a local minimum and thereupon exhibits a sharp rise up to the top end. Also, the heat transfer profiles show a similar variation trend with time, as indicated by shifting upward till the end of the first quarter of the cycle and then downward of the location where the local minimum heat transfer arises. This non-monotonic temporal behavior as shall be demonstrated in Fig. 6 is primarily due to growing and decaying of a clockwise secondary recirculation adjacent to the hot wall, related to density inversion phenomenon, in response to the sinusoidal modulation of the hot wall temperature.

The periodic progression of the buoyant flow field in the water region and the temperature distribution inside the enclosure during the steady periodic melting regime for $Ste = 0.051$, $Sc = 0.25$, $Ra = 10^6$, $p = 0.5$, and $A = 1.0$ is illustrated by the contour plots of streamlines (left) and isotherms (right) in Fig. 6. In the contour plots, the hot wall of the enclosure is on the left, and the ice–water interface is traced by a dot dashed line. In addition, the isotherm contour for the maximum density, $\theta = R$, is denoted by a dashed line, if it exists. Having the density maximum located near the hot wall during the first and second quarter of the cycle, the buoyancy-driven flow field in the water region, as displayed in Figs. 6(a)–(e), evolves from a convective inversion flow pattern at the beginning of the cycle into one featuring a dominant counterclockwise recirculation demarcated along the density-extreme isotherm with a contra-rotating secondary eddy, growing and decaying in accordance with the sinusoidal rise and fall of the hot wall temperature. With further decline of the hot wall temperature below 4°C through the third quarter of the cycle, the counterclockwise melt flow appears to be gradually impeded due to the growing contra-rotating eddy near the hot wall so that a bicellular flow pattern of nearly equal strength arises at the end the third quarter as shown in Fig. 6(g). Moreover, from the isotherms in Fig.

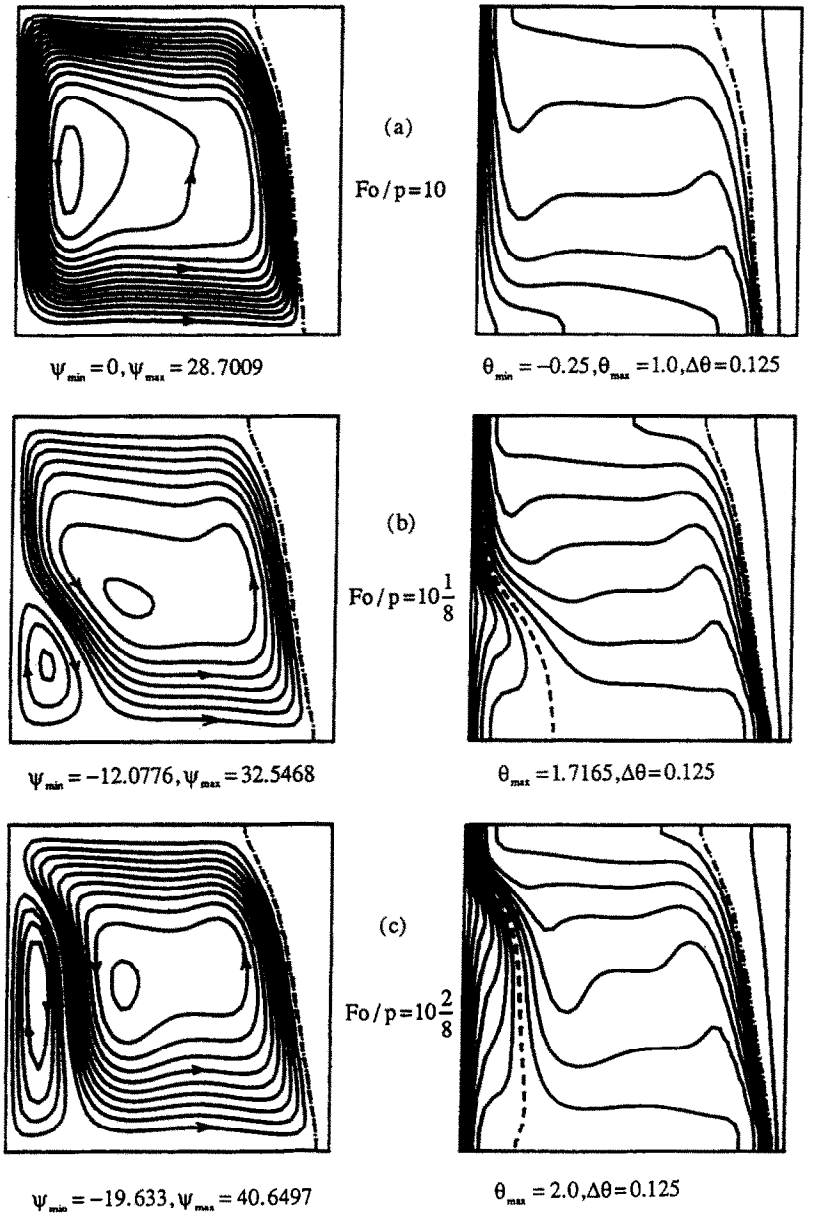

FIG. 6. Cyclic development of flow structure (left) and temperature distribution (right) during steady periodic melting process of ice for $Ste = 0.051$, $Sc = 0.25$, $p = 0.5$, $A = 1.0$ and $Ra = 10^6$.

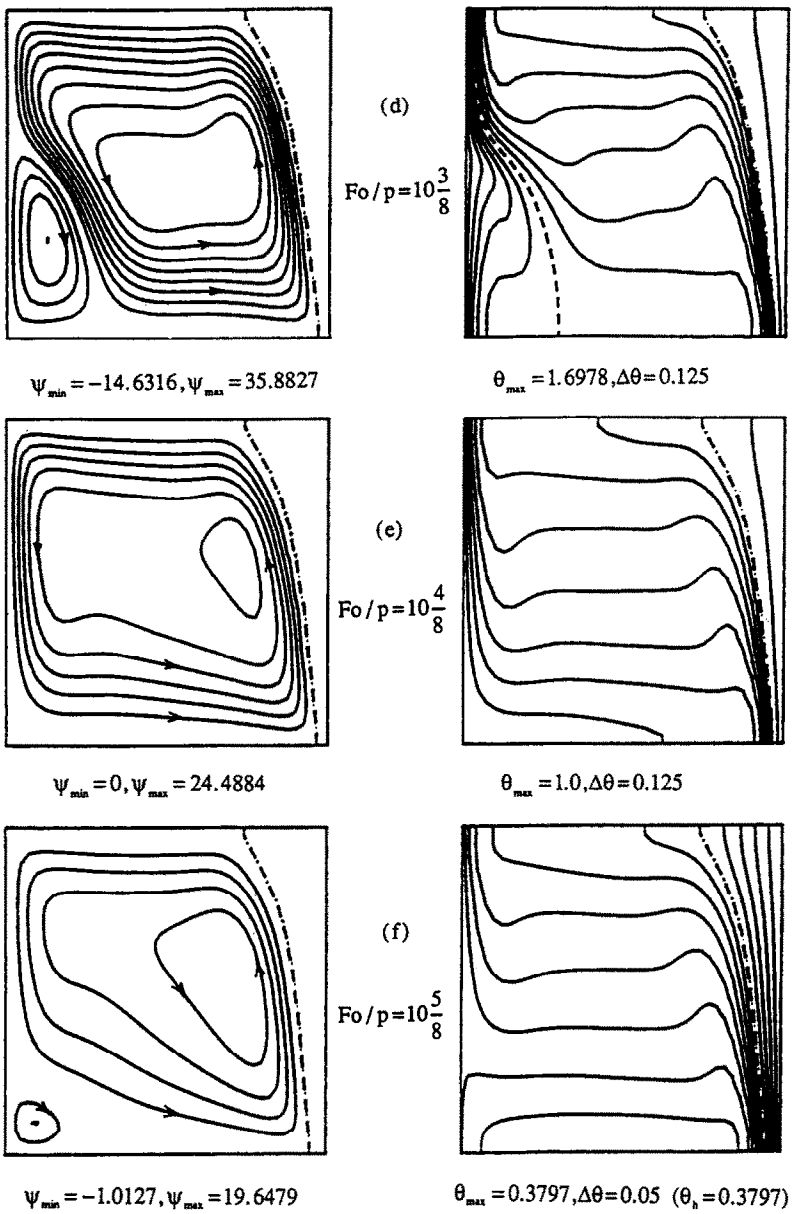

FIG. 6.—*Continued.*

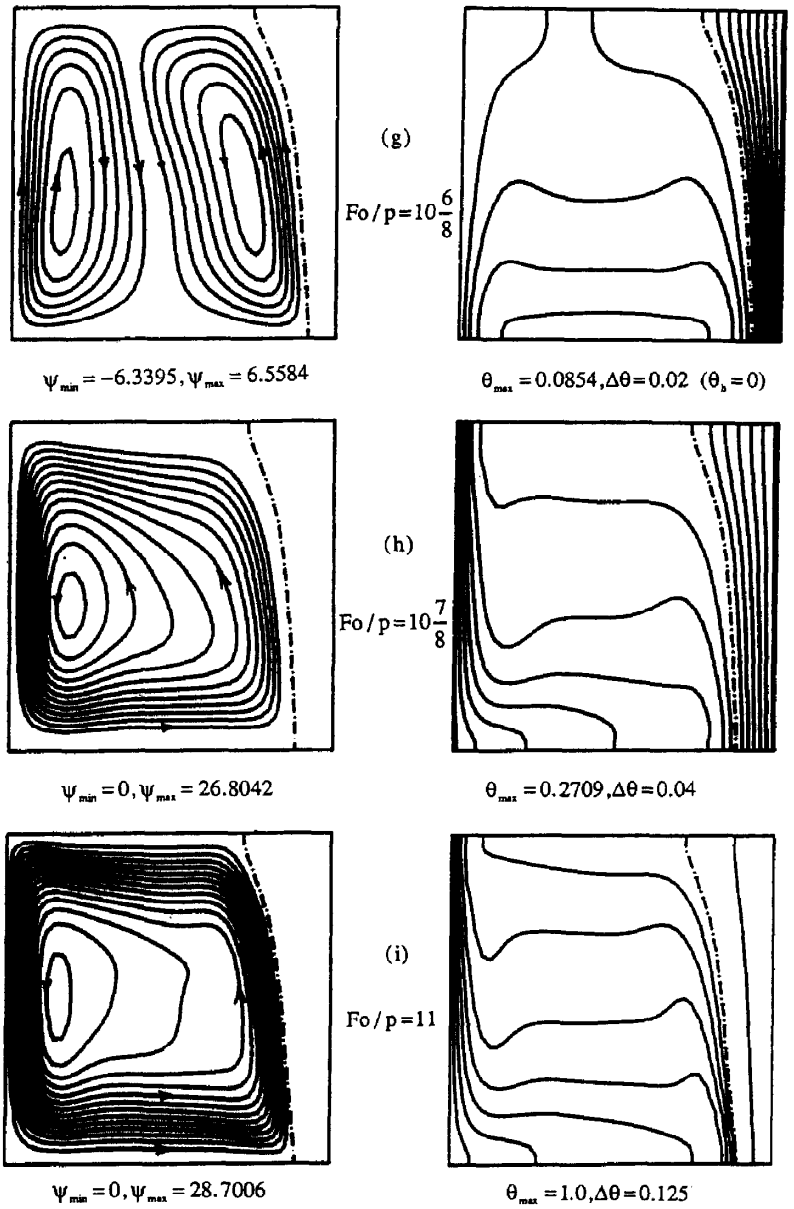

FIG. 6.—*Continued.*

6(f), a pocket of warmer water at temperature higher than the hot wall can be detected staying in the bottom region of the melt. At the end of the third quarter, the melt zone is virtually at a temperature higher than the hot wall (Fig. 6(g)), thus rendering a back heat flow from the melt zone toward the hot wall of the enclosure, as indicated by the slightly negative values of $\bar{Q}_h$ in Fig. 4 at the corresponding instant of time. Then, as the hot wall temperature rises back to 4°C through the fourth quarter, the streamline pattern as well as the isotherm distribution evolves back to that observed at the beginning of the cycle. The above-elaborated cyclic variation of the buoyant convection in the melt region flow is in the sense of convection opposite to that of the pure tin observed in ref. [9], a clear indication of the convective inversion due to the density inversion phenomenon in the melt.

For higher $Ste = 0.101$ ($\bar{T}_h = 8°C$), the increase of the imposed oscillation amplitude of the hot wall temperature exerts an influence somewhat opposite to that found for $Ste = 0.051$ on the heat transfer and the melted fraction of ice in the enclosure. As revealed in Fig. 7 for $Ste = 0.101$, $Ra = 10^6$, $Sc = 0.25$, and $p = 0.5$, the imposed time-periodic oscillatory hot-surface temperature with increasing amplitude tends to yield great enhancement of the melted fraction and the heat transfer rates, as compared with that under

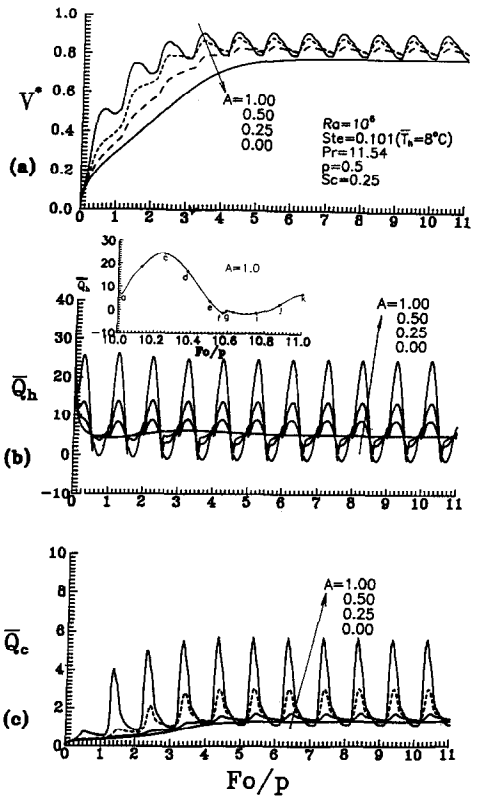

FIG. 7. Effect of oscillation amplitude on temporal variation of melted fraction and heat transfer rates at the vertical walls for $Ste = 0.101$.

static condition ($A = 0$). This clearly reflects the feasibility of enhancing heat transfer during the melting process of ice through the temporally sinusoidal perturbation on the hot wall temperature, which was not found for tin [9]. Further scrutiny of the heat transfer histories at the hot wall for $Ste = 0.101$ presented in Fig. 7(b) reveals a more complex variation with time than those of $Ste = 0.051$ in Fig. 4(b). This is due to a further pronounced temporally changing flow structure related to density inversion.

Figure 8 exemplifies the cyclic evolution of the flow structure and the temperature distribution at the instants of time denoted in the inset of Fig. 7(b) during the steady periodic melting regime of ice for $Ste = 0.101$. The cycle starts with a flow pattern dominated by a counterclockwise circulation near the ice front, which is then drastically suppressed by the rapidly intensified clockwise cell near the hot wall in response to the rising hot wall temperature through the first quarter of the cycle. At the end of the first quarter, as shown in Fig. 8(c), the flow structure as well as the temperature field in the melt zone is reverted to the one controlled by the clockwise recirculating flow. Driven by the sinusoidal drop of the hot wall temperature through the second quarter, the dominance of the clockwise flow structure is then fading away progressively in the presence of growing contra-rotating eddy adjacent to the ice front (see Figs. 8(d) and (e)). With continuing decline of the hot wall temperature below 8°C, the flow field in the melt exhibits a drastic change of recirculation pattern; as illustrated in Fig. 8(f) the counterclockwise recirculation near the ice front becomes the dominant flow structure in the melt region. Further from the isotherm of Fig. 8(f), a pocket of warmer melt at temperature higher than the hot wall can be discerned floating in the top left corner of the enclosure, indicative of a back heat flow phenomenon there. Through the first half of the third quarter of cycle, Figs. 8(f)–(h), the occurrence of the local back heat flow continues but shifts downward to the bottom, a pocket of the warmer melt settling down to the floor of the enclosure. At the end of the third quarter, resembling the case of $Ste = 0.051$ in Fig. 6, a bicellular flow structure prevails in the melt region. Then, during the final quarter of the cycle, the flow structure displays another cycle of growing and decaying of a counterclockwise secondary eddy at the bottom left corner of the melt zone.

In Fig. 9, the periodic mean values and the induced oscillation amplitudes of the melted fraction of ice and the heat transfer rates at the vertical walls during the steady period melting regime are plotted against the forcing oscillation amplitude of the hot-wall temperature. Note that the induced oscillation amplitude presented in Fig. 9 is evaluated as half of the difference between the maximum and minimum values of the oscillatory quantity of interest over a cycle of the steady periodic melting process. In conformity with the aforementioned, the effects of the forcing oscillation

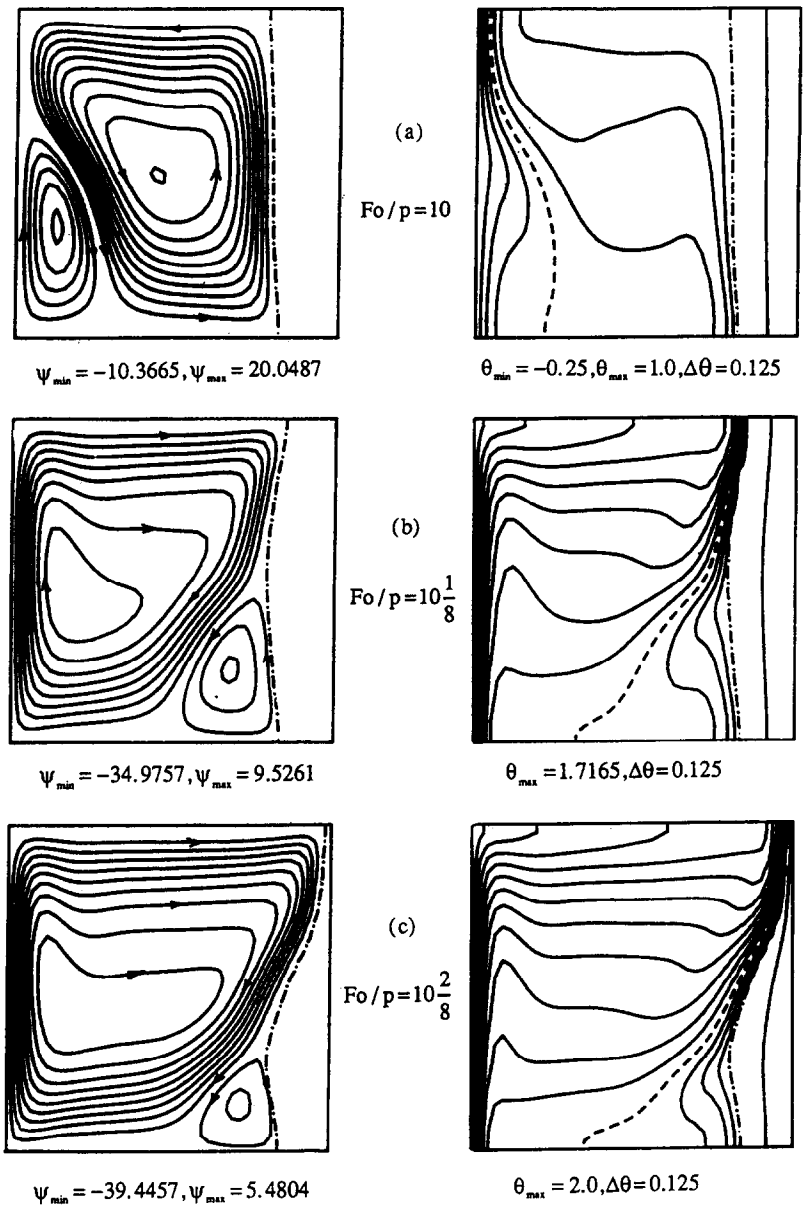

FIG. 8. Cyclic progression of flow structure and temperature distribution during the steady periodic melting process of ice for $Ste = 0.101$.

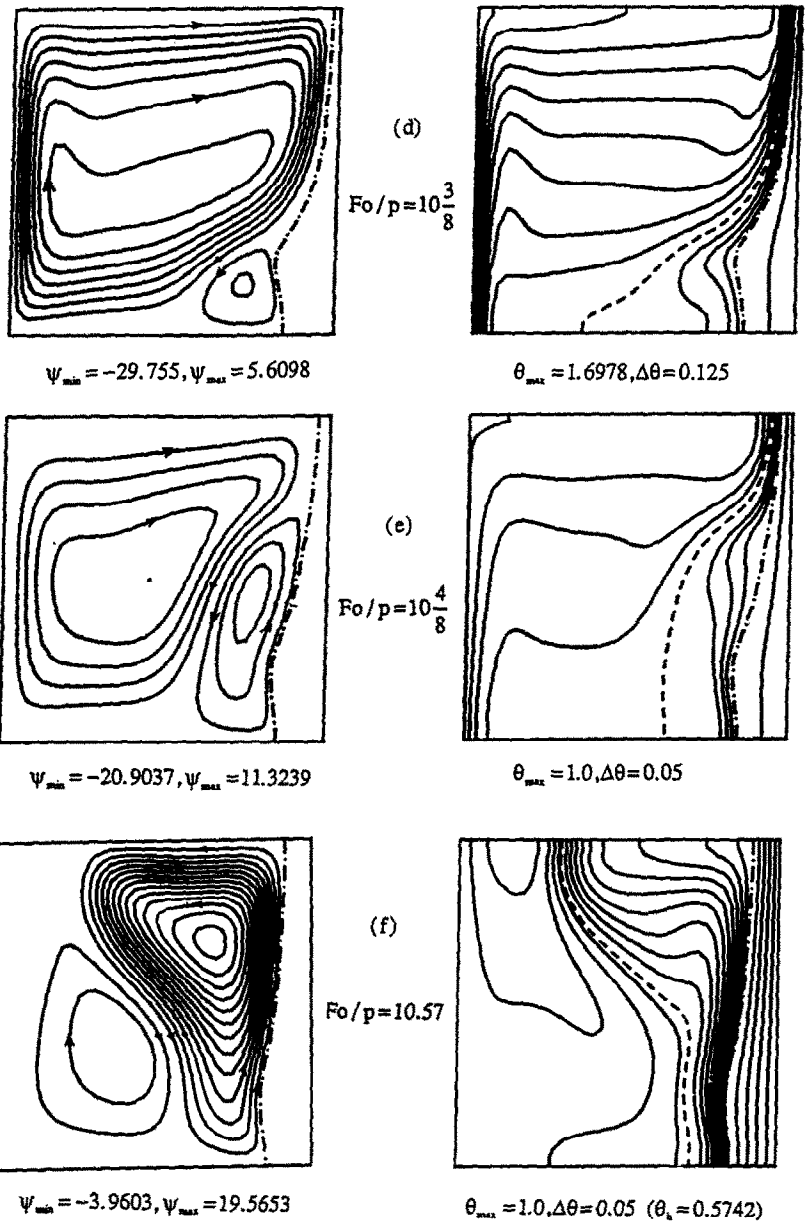

FIG. 8.—*Continued.*

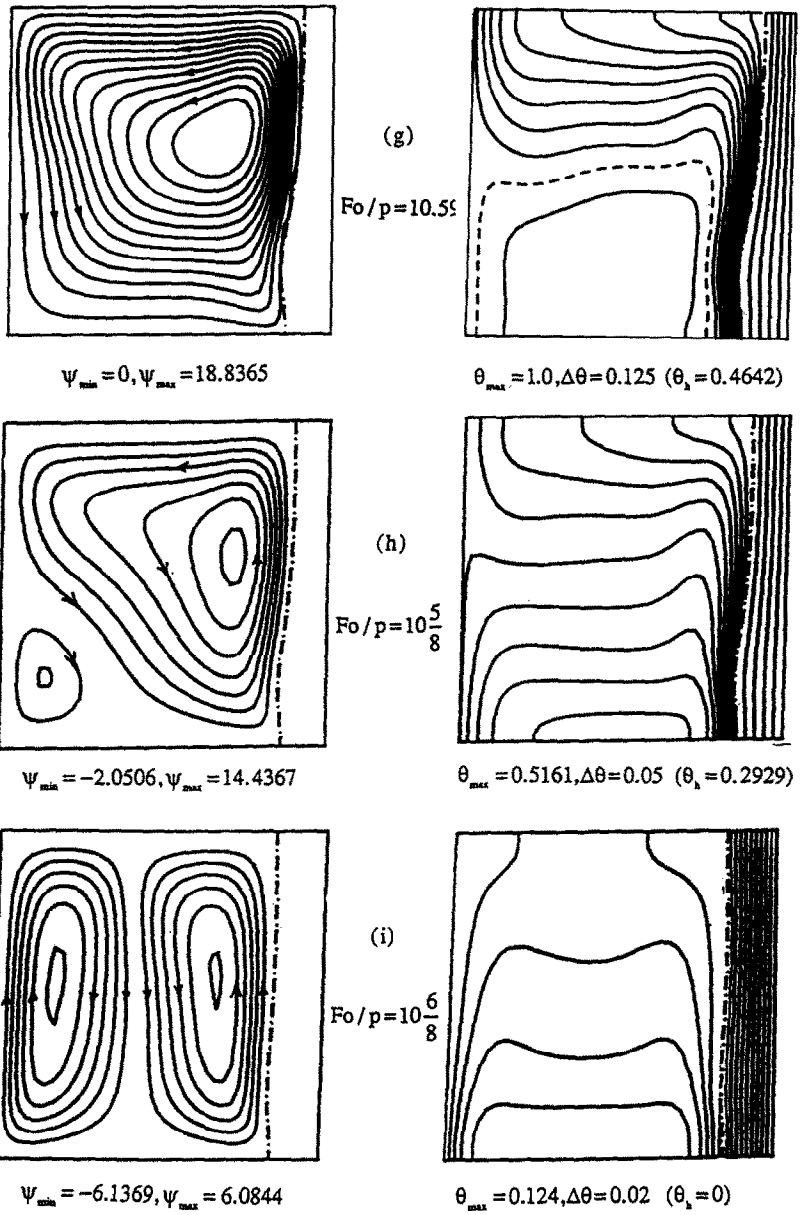

FIG. 8.—*Continued.*

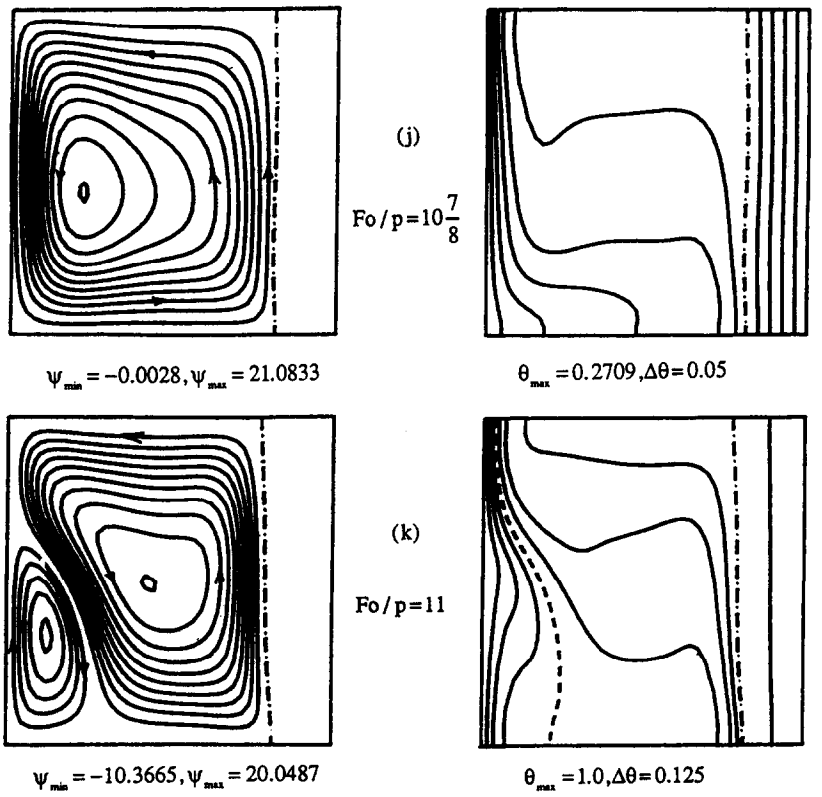

FIG. 8.—*Continued.*

amplitude are a strong function of the Stefan number related to density anomaly of water. From Fig. 9 it can be seen that the periodic mean value of $\bar{Q}_h$ increases with the imposed oscillation amplitude for $Ste = 0.101$, while the opposite occurs for $Ste = 0.051$. Furthermore, a quasi-linear amplitude response to the increasing temperature oscillation amplitude imposed on the hot wall can be observed for the heat transfer rates through the vertical walls as well as the melted fraction of ice. The induced oscillation amplitudes of $\bar{Q}_h$, $\bar{Q}_c$ and V^* appear to be further amplified for $Ste = 0.101$ in comparison with those of $Ste = 0.051$.

Effect of time period

The increase of the time period of the sinusoidal hot wall temperature tends to delay the onset of the steady periodic melting regime but induces marked amplification of the induced oscillation amplitudes of both the melted fraction and heat transfer rate at the

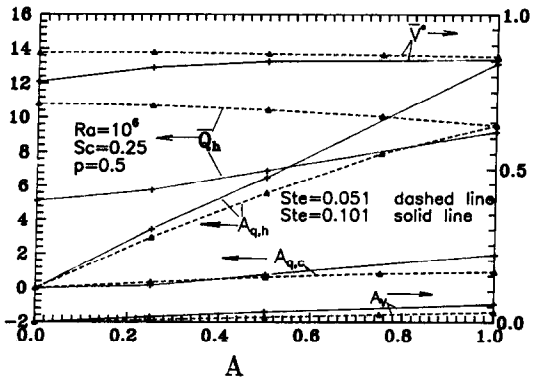

FIG. 9. Dependence of periodic mean values and induced oscillation amplitudes of melted fraction and heat transfer rates at the vertical walls on the imposed oscillation amplitude.

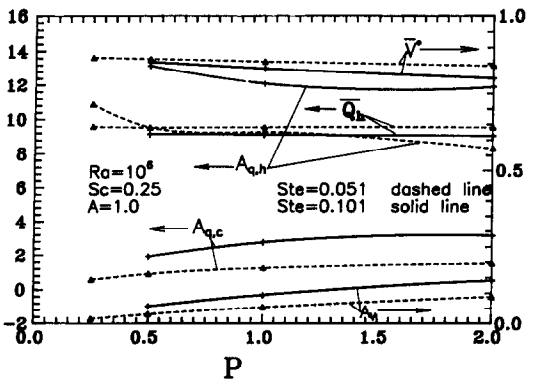

FIG. 10. Effect of time period on the average mean values and induced oscillation amplitudes of melted fraction of ice and heat transfer rates during steady periodic melting regime.

cold wall. Adversely, the increase of the time period results in slightly lower oscillation amplitude of heat transfer at the hot wall. The effects of varying time period become further pronounced at $Ste = 0.101$. Figure 10 further quantifies the foregoing effects of the time period. The periodic mean value of the melted fraction shows a decreasing trend with increasing time period of the sinusoidal hot wall temperature. Moreover, the periodic-averaged heat transfer rate at the hot wall appears to be rather insensitive to the variation of the time period.

Effect of Rayleigh number

The increase of Ra for fixed values of the other parameters greatly amplifies the oscillatory behavior of heat transfer rates at the vertical walls, as indicated by the increasing induced oscillation amplitudes of the heat transfer rates as well as the melted fraction of ice shown in Fig. 11. Relatively, the melted fraction responds to the increasing Ra with a slightly higher-amplitude oscillation. Moreover, the periodic mean values of V^* and $\bar{Q}_h$ display a drastic increase with the increase of Ra, further indication of the dominant role of natural convection in the melting process. Another interesting trend that can be detected in Fig. 11 is that the dependence of the periodic mean value of V^* on Ste appears to diminish at high $Ra = 10^6$.

Effect of subcooling parameter

Next, the effect of the subcooling parameter is considered. Lower subcooling, as expected, leads to great enhancement of the melted fraction of ice. Quantitatively, as illustrated in Fig. 12, the increase of Sc causes great reduction in the periodic mean melted fraction, but exerts a relatively minute influence on the induced oscillation amplitude as well as the periodic mean value of the heat transfer rate. Moreover, an effect of Sc resembling that found in ref. [9] for pure tin on the heat transfer rate through the cold wall is detected for the melting process of ice as well. Following a certain period of the melting process, the influence of Sc on $\bar{Q}_c$ is reversed that lower Sc results

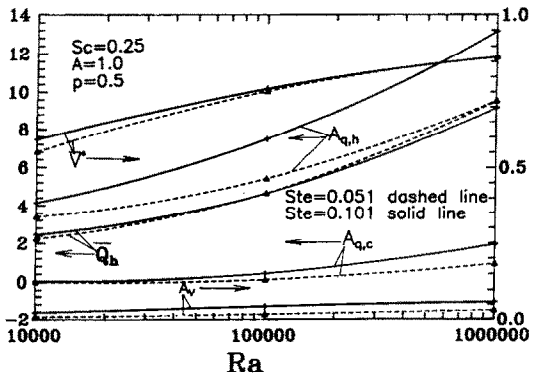

FIG. 11. Effect of Ra on mean values and oscillation amplitudes of melted fraction and heat transfer rates.

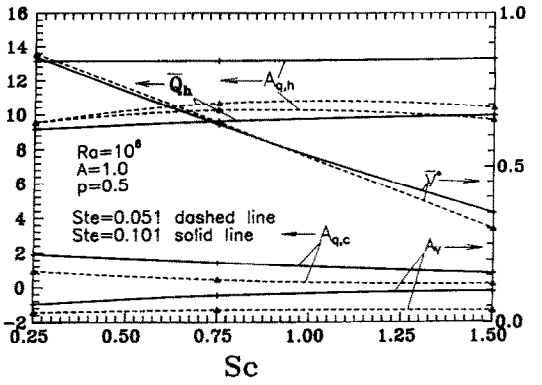

FIG. 12. Influence of subcooling parameter on mean values and oscillation amplitudes of melted fraction and heat transfer rates.

in higher-amplitude oscillation of $\bar{Q}_c$, as presented in Fig. 12. Above all, the foregoing effect of the subcooling parameter on the heat transfer rates and the melted fraction of ice exhibits a dependence on the Stefan number as well.

Correlation

Finally, correlation for the results of the periodic mean values and the oscillation amplitudes of the melted fraction of ice and the heat transfer rates during the steady periodic melting regime for $Ste = 0.051$ and 0.101 has been generated via the least square regression analysis. For $Ste = 0.051$, $A = 0.25 \sim 1.0$, $p = 0.25 \sim 2.0$, $Ra = 10^4 \sim 10^6$, and $Sc = 0.25 \sim 1.50$:

$$\bar{V}^* = 0.280 A^{-0.006} p^{-0.019} Ra^{0.092} \left(\frac{Sc^{0.073}}{1+Sc^{2.21}}\right) \tag{10a}$$

with the maximum and average deviation of 6.43 and 1.32%, respectively; and

$$\bar{Q}_h = 0.114 A^{-0.054} p^{-0.046} Ra^{0.325} Sc^{0.035} \tag{10b}$$

with the maximum and average deviation of 4.58 and 1.72%, respectively.

$$A_c = 0.006 A^{1.041} \left(\frac{p^{1.151}}{1+p^{0.834}}\right) Ra^{0.278} \left(\frac{Sc^{0.477}}{1+Sc^{1.028}}\right) \tag{10c}$$

with the maximum and average deviation of 5.26 and 1.54%, respectively; and

$$A_{q,h} = 0.614 A^{0.855} p^{-0.121} \left(\frac{1+Ra^{0.071}}{Ra^{-0.071}-0.256}\right) \times \left(\frac{Sc^{0.345}}{1+Sc^{0.833}}\right) \tag{10d}$$

with the maximum and average deviation of 7.62 and

2.78%, respectively; and

$$A_{q,c} = 0.031\left(\frac{A^{1.127}}{1+A^{1.621}}\right)\left(\frac{p^{0.891}}{1+p^{1.076}}\right) \times\left(\frac{1+Ra^{1.170}}{Ra^{0.559}+872.2}\right)\left(\frac{Sc^{-0.380}}{1+Sc^{1.346}}\right) \quad (10e)$$

with the maximum and average deviation of 1.81 and 0.52%, respectively. For $Ste = 0.101$, $A = 0.25 \sim 1.0$, $p = 0.25 \sim 1.0$, $Ra = 10^4 \sim 10^6$, and $Sc = 0.25 \sim 1.50$:

$$\bar{V}^* = 0.338A^{0.038}p^{-0.066}Ra^{0.080}\left(\frac{Sc^{0.083}}{1+Sc^{1.79}}\right) \quad (11a)$$

with the maximum and average deviation of 4.52 and 1.54%, respectively; and

$$\bar{Q}_h = 0.197A^{0.332}p^{0.005}Ra^{0.283}Sc^{0.056} \quad (11b)$$

with the maximum and average deviations of 3.24 and 1.04%, respectively.

$$A_r = 7.567A^{0.855}p^{0.640}\left(\frac{1+Ra^{0.414}}{2753+Ra^{0.620}}\right)\left(\frac{Sc^{0.629}}{1+Sc^{0.828}}\right) \quad (11c)$$

with the maximum and average deviation of 3.93 and 1.76%, respectively; and

$$A_{q,h} = 0.398A^{0.966}p^{-0.073}Ra^{0.250}Sc^{0.006} \quad (11d)$$

with the maximum and average deviation of 2.62 and 1.14%, respectively; and

$$A_{q,c} = 23.5\left(\frac{A^{2.236}}{1+A^{5.090}}\right)\left(\frac{p^{1.055}}{1+p^{1.411}}\right) \times\left(\frac{1+Ra^{1.054}}{1\,167\,600+Ra^{1.066}}\right)\left(\frac{Sc^{0.076}}{1+Sc^{1.724}}\right) \quad (11e)$$

with the maximum and average deviation of 0.05 and 0.01%, respectively.

CONCLUDING REMARKS

A numerical study has been carried out to investigate the natural-convection-dominated melting process of ice from a vertical wall with time-dependent sinusoidal temperature perturbation inside a square enclosure. Similar to the findings in ref. [9] for pure tin as PCM, a steady-periodic melting regime of ice at the frequency of the imposed time-periodic perturbation on the surface temperature emerges after a transient oscillatory melting process. The synchronous response of the melting process of ice to the time-periodic temperature perturbation is strongly affected by the density inversion phenomenon of water near 4°C. In contrast to the melting process of the pure tin considered in ref. [9], results from the present simulations demonstrate that the time-periodic temperature perturbation imposed on the vertical hot wall in conjunction with the density inversion effect of water can be a viable means for controlling melting heat transfer in an ice-filled enclosure. For $Ste = 0.101$ ($\bar{T}_h = 8°C$) the increase of the amplitude of the forcing oscillatory hot-wall temperature greatly enhances the melting heat transfer across the enclosures as well as the melted fraction of ice during the steady periodic melting regime. On the other hand, an adverse effect for the increasing oscillation amplitude of hot wall temperature is found for $Ste = 0.051$ ($\bar{T}_h = 4°C$). Moreover, the heat transfer rates through the vertical walls as well as the melted fraction of ice during the steady periodic melting regime are strongly influenced by the Rayleigh number, further indicating the predominant role of the buoyant flow in the melting process of ice. The higher subcooling parameter leads to greatly reduced periodic mean melted fraction of ice but with a higher-amplitude oscillation. The periodic mean value of the heat transfer rate is rather insensitive to the variation of the time period of the forcing wall temperature oscillation and of the subcooling parameter.

REFERENCES

1. R. Viskanta, Phase-change heat transfer. In *Solar Heat and Storage: Latent Heat Materials* (Edited by G. A. Lane), pp. 153–222. CRC Press, Boca Raton, Fl. (1983).
2. R. Viskanta, Natural convection in melting and solidification. In *Natural Convection: Fundamentals and Applications* (Edited by S. Kakac *et al.*), pp. 845–877. Hemisphere, Washington D.C. (1985).
3. R. Viskanta, Heat transfer during melting and solidification of metals, *J. Heat Transfer* **110,** 1205–1219 (1988).
4. N. W. Hale, Jr. and R. Viskanta, Photographic observation of the solid–liquid interface motion during melting of a solid heated from an isothermal vertical wall, *Lett. Heat Mass Transfer* **5,** 329–337 (1978).
5. C. J. Ho and R. Viskanta, Heat transfer during melting from an isothermal vertical wall, *J. Heat Transfer* **106,** 12–19 (1984).
6. M. Okada, Analysis of heat transfer during melting from a vertical wall, *Int. J. Heat Mass Transfer* **27,** 2057–2066 (1984).
7. C. Bénard, C. Gobin and F. Martinez, Melting in a rectangular enclosure: experiments and numerical simulations, *J. Heat Transfer* **107,** 794–803 (1985).
8. Z. Zhang and A. Bejan, Melting in an enclosure heated at constant rate, *Int. J. Heat Mass Transfer* **32,** 1063–1076 (1989).
9. C. J. Ho and C. H. Chu, Periodic melting within a square enclosure with an oscillatory surface temperature, *Int. J. Heat Mass Transfer* **36,** 725–733 (1993).
10. J. Hermann, W. Leidenfrost and R. Viskanta, Melting of ice around a horizontal isothermal cylindrical heat source, *Chem. Engng Commun.* **25,** 63–78 (1984).
11. D. White, R. Viskanta and W. Leidenfrost, Heat transfer during the melting of ice around a horizontal, isothermal cylinder, *Experiments in Fluids* **4,** 171–179 (1986).
12. C. J. Ho and S. Chen, Numerical simulation of melting of ice around a horizontal cylinder, *Int. J. Heat Mass Transfer* **29,** 1359–1369 (1986).

13. H. Rieger and H. Beer, The melting process of ice inside a horizontal cylinder: effects of density anomaly, *J. Heat Transfer* **108,** 166–173 (1986).
14. B. W. Webb, M. K. Moallemi and R. Viskanta, Experiments on melting of unfixed ice in a horizontal cylindrical capsule, *J. Heat Transfer* **109,** 454–459 (1987).
15. B. Gebhart and J. Mollendorf, A new density relation for pure and saline water, *Deep Sea Res.* **24,** 831–848 (1977).
16. P. J. Roache, *Computational Fluid Dynamics*. Hermosa, Albuquerque, New Mexico (1976).
17. S. L. Lee and R. Y. Tzong, An enthalpy formulation for phase change problem with a large thermal diffusivity jump across the interface, *Int. J. Heat Mass Transfer* **34,** 1491–1502 (1991).
18. W. Y. Raw and S. L. Lee, Application of weighting function scheme on convective–conduction phase change problems, *Int. J. Heat Mass Transfer* **34,** 1503–1513 (1991).
19. D. A. Anderson, J. C. Tannehill and R. H. Pletcher, *Computational Fluid Mechanics and Heat Transfer*. Hemisphere, Washington D.C. (1984).
20. R. Viskanta and F. Wolff, Melting of a pure metal from a vertical wall, *Experimental Heat Transfer* **1,** 17–30 (1987).
21. C. Bénard and D. Gobin, Numerical simulation of melting process for metals. In *Multiphase Flow, Heat and Mass Transfer*, ASME HTD-Vol. 109, pp. 55–60. ASME, New York (1989).
22. G. de Vahl Davis, E. Leonardi, P. H. Wong and G. H. Yeoh, Natural convection in a solidifying liquid, *The Sixth International Conference for Numerical Methods in Thermal Problems*, pp. 410–420. Pinerridge, Swansea (1989).